Mass production and dynamic imaging of fluorescent nanodiamonds

YI-REN CHANG[1†], HSU-YANG LEE[1†], KOWA CHEN[1], CHUN-CHIEH CHANG[2], DUNG-SHENG TSAI[1], CHI-CHENG FU[1], TSONG-SHIN LIM[1‡], YAN-KAI TZENG[1], CHIA-YI FANG[1,3], CHAU-CHUNG HAN[1], HUAN-CHENG CHANG[1,3]* AND WUNSHAIN FANN[1,2,4]*

[1]Institute of Atomic and Molecular Sciences, Academia Sinica, Taipei 106, Taiwan
[2]Department of Physics, National Taiwan University, Taipei 106, Taiwan
[3]Department of Chemistry, National Taiwan Normal University, Taipei 106, Taiwan
[4]Institute of Polymer Science and Engineering, National Taiwan University, Taipei 106, Taiwan
[†]These authors contributed equally to this work
[‡]Present address: Department of Physics, Tunghai University, Taichung 407, Taiwan
*e-mail: fann@gate.sinica.edu.tw; hcchang@po.iams.sinica.edu.tw

Published online: 27 April 2008; doi:10.1038/nnano.2008.99

Fluorescent nanodiamond is a new nanomaterial that possesses several useful properties, including good biocompatibility[1], excellent photostability[1,2] and facile surface functionalizability[2,3]. Moreover, when excited by a laser, defect centres within the nanodiamond emit photons that are capable of penetrating tissue, making them well suited for biological imaging applications[1,2,4]. Here, we show that bright fluorescent nanodiamonds can be produced in large quantities by irradiating synthetic diamond nanocrystallites with helium ions. The fluorescence is sufficiently bright and stable to allow three-dimensional tracking of a single particle within the cell by means of either one- or two-photon-excited fluorescence microscopy. The excellent photophysical characteristics are maintained for particles as small as 25 nm, suggesting that fluorescent nanodiamond is an ideal probe for long-term tracking and imaging *in vivo*, with good temporal and spatial resolution.

Serving as an *in vivo* nanoprobe, fluorescent nanodiamonds (FNDs) have two major advantages over the commonly used fluorescent beads[5] and quantum dots[6,7]. First, the emission from FNDs is exceptionally stable; no photobleaching or fluorescence intermittency are observed, even for a single nitrogen vacancy (N-V) defect centre[8,9]. Second, diamond nanoparticles are non-toxic to a number of cell types, as has been documented by cell viability assays[1,10–13]. In recent work[7], the axonal transport of nerve growth factor signals was studied using quantum dots for live tracking. It was found that dots made of materials such as CdSe were immune to photobleaching in live cells; however, the photoblinking characteristic of these semiconductor fluorophores rendered their utility for continuous three-dimensional tracking difficult. In contrast, FND is perfectly photostable, allowing the tracking and imaging of a single FND particle in a cell for hours.

Although FNDs are well suited for biomedical use, the nanomaterial has not yet received widespread exploitation because of difficulties in its mass production. Conventionally, the N-V defect centres in diamond are produced by bombarding the material with a high-energy (typically 2 MeV) electron beam from a van de Graaff accelerator, followed by annealing at elevated temperatures (typically 800 °C)[4,8,9,14,15]. This requires highly sophisticated and costly equipment, which therefore hinders the easy availability of FNDs. We present a practical method to scale up the production of FNDs using a home-built prototype device composed of a high-fluence, medium-energy He^+ beam. Compared with previously used methods[1,2], the setup has boosted FND yield by nearly two orders of magnitude and can be installed and operated safely in ordinary laboratories.

High-brightness FNDs were produced through radiation-damage of synthetic type Ib diamond powders (mean sizes of 35 and 140 nm) using 40-keV He^+ bombardment at a dose of $\sim 1 \times 10^{13}$ ions cm^{-2}. The merit of using He^+ as the damage agent is threefold. First, helium atoms are chemically inert, and embedding these atoms in a diamond lattice through neutralization of the stopped He^+ ions does not appreciably change the photophysical properties of the FNDs produced. Second, a 40-keV He^+ ion can create 40 vacancies as it penetrates diamond[16], in contrast to the 0.1 and 13 vacancies generated by 2-MeV e^- and 3-MeV H^+, respectively[15,17]. This remarkably high damaging efficacy reduces the ion dosage required for irradiation. Third, high-fluence 40-keV He^+ beams can be readily generated by radio-frequency ion sources. The current typically delivered by these sources is $\sim 10\ \mu A$ ($\sim 6 \times 10^{13}$ ions s^{-1}), which is more than two orders of magnitude higher than that of a 3-MeV H^+ beam emanating from a tandem particle accelerator[1,17]. These factors together make it possible and practical to produce bright FNDs on a large scale (see Supplementary Information, Figs S1 and S2).

Figure 1a shows an ensemble emission spectrum ($\lambda_{max} =$ 680 nm) of 35-nm FNDs prepared by He^+ irradiation. The spectrum, acquired for particles suspended in water (inset in Fig. 1a) and excited with a continuous-wave (cw) 532-nm laser (see Supplementary Information, Fig. S3), reveals two types of N-V centres inside the material: $(N\text{-}V)^0$ with a zero-phonon line at 575 nm and $(N\text{-}V)^-$ with a zero-phonon line at 638 nm (ref. 14) Comparing it with the spectrum of another sample

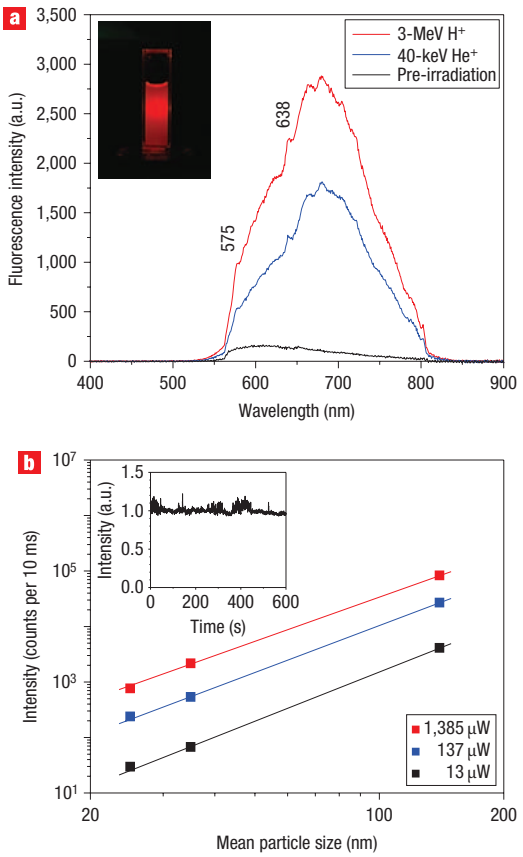

Figure 1 Characterization of FNDs. a, Fluorescence spectra of 35-nm FNDs suspended in water (1 mg ml^{-1} each), prepared with either 40-keV He^+ or 3-MeV H^+ irradiation. Inset: Fluorescence image of a 35-nm FND suspension excited by 532-nm laser light. **b**, Fluorescence intensities of FNDs as a function of particle size at three different laser powers. Each data point is the mean of measurements for more than 15 different FNDs. The slopes of the linear fits vary from 2.65 to 2.95 over the power range used in the measurements. Inset: Fluorescence time trace (intensity normalized) of a 25-nm FND.

damaged by 3-MeV protons at a dose of $\sim 1 \times 10^{16}$ H^+ cm^{-2} indicates that the fluorescence spectra of the FNDs prepared under these two drastically different bombardment conditions are essentially the same, except that their intensities differ by ~30%. As the concentration of the $(N\text{-}V)^-$ centres created by 3-MeV H^+ irradiation has been previously quantified to be ~25 p.p.m. for type Ib diamond single crystals[17], the spectral comparison here provides an estimate that the FNDs prepared by the 40-keV He^+ irradiation contain more than 10 p.p.m. of the $(N\text{-}V)^-$ centres. In contrast, the sample without irradiation has an $(N\text{-}V)^-$ concentration much less than 1 p.p.m.

Producing large quantities of FNDs with He^+ beam irradiation allows us to extract smaller diamond nanoparticles from the 35-nm ensembles by repeated centrifugal fractionation. The particles so extracted have a mean size of 25 nm, as revealed by both transmission electron microscopy (TEM) and dynamic light scattering measurements (see Supplementary Information, Figs S4 and S5). Figure 1b shows the fluorescence intensity of these particles together with those of 35-nm and 140-nm FNDs following one-photon excitation (OPE) at 532 nm. The observed signals scale nearly linearly with the volumes of the particles excited at three different laser energies, indicating that the fluorescence intensities of these FNDs are bulk-dependent, little affected by their surface characteristics and, therefore, their environments. Notably, the excellent photostability (that is, no photobleaching or photoblinking) of the material is preserved even for particles as small as 25 nm (inset, Fig. 1b).

Apart from exhibiting excellent OPE photostability, the FNDs also show similarly good properties under two-photon excitation (TPE)[18,19]. Figure 2a presents a confocal scanning TPE fluorescence image of 140-nm FNDs dispersed on a cover-glass slide and excited by a femtosecond laser operated at 875 nm. In the image, the cross-sections of the individual spots have a full-width at half-maximum of ~300 nm, very close to the theoretical diffraction limit of the optical microscope. A laser power dependence measurement of the fluorescence intensity confirmed that the 875-nm excitation is indeed a two-photon process (see Supplementary Information, Fig. S6a). Because the TPE matches better with the absorption band of the $(N\text{-}V)^0$ centres than that of $(N\text{-}V)^-$(ref. 20), it produces a spectrum markedly blueshifted from the corresponding OPE spectrum acquired at 532 nm, where the $(N\text{-}V)^-$ centres were predominantly excited (Fig. 2b)[14,20]. In accord with the earlier observations[21] some $(N\text{-}V)^-$ centres were irreversibly converted to $(N\text{-}V)^0$ due to ionization by the femtosecond laser illumination (see Supplementary Information, Fig. S6b). Similar to the OPE of $(N\text{-}V)^-$, neither photobleaching nor photoblinking was observed in the TPE emission of $(N\text{-}V)^0$ after prolonged (>10 min) excitation of the individual 35-nm and 140-nm FND particles (Fig. 2c).

As an imaging technique for biomedical use, TPE microscopy outperforms OPE microscopy in one important aspect, in that it generates better contrast images owing to the marked reduction of autofluorescence and light scattering background signals from the specimen[18,19,22]. This outstanding performance is demonstrated here with FNDs. Figure 3a displays confocal scanning images of a fixed HeLa cell after uptake of 140-nm FNDs and probing with both OPE and TPE microscopies. The three images in each column are axial slices of the cell acquired at three different positions in each excitation, showing the cellular uptake of the particles (labelled with red and yellow boxes). A comparison between the results of these two excitations clearly indicates that the TPE provides significantly better contrast images. Using the residual background signals from light scattering and cell autofluorescence, we reconstructed a three-dimensional image of the cell, as shown in Fig. 3b. No evidence was found for the entry of the particle into the nucleus (see Supplementary Information, Movie S1). To provide a more quantitative assessment for the contrast improvement, we analysed the intensity profile of one of the FNDs in the cytoplasm (Fig. 3c) and determined that both the lateral and axial cross-sections of the TPE images are only half those of the corresponding OPE images. Such a noticeable difference in resolution between these two excitations, particularly in the axial direction, is attributed to the fact that our measurement used an optical fibre with an aperture of 200 μm, which significantly degraded the spatial resolution of the OPE due to the collection of signals from off-focus excitation in a highly scattering environment such as the cell cytoplasm[22].

The excellent photostability and high brightness of the material also make long-term, three-dimensional tracking[23–25] of a single FND in a live cell possible. The technique holds great promise for revealing details of intracellular activities such as drug delivery and virus infection[26]. Figure 4a displays the bright-field and OPE fluorescence images of a live HeLa cell after uptake of 35-nm FNDs. The uptake of the FND particles was, again, confirmed by axial sectioning of the cell[2]. By using a home-built servo control system and operating the fluorescence microscope

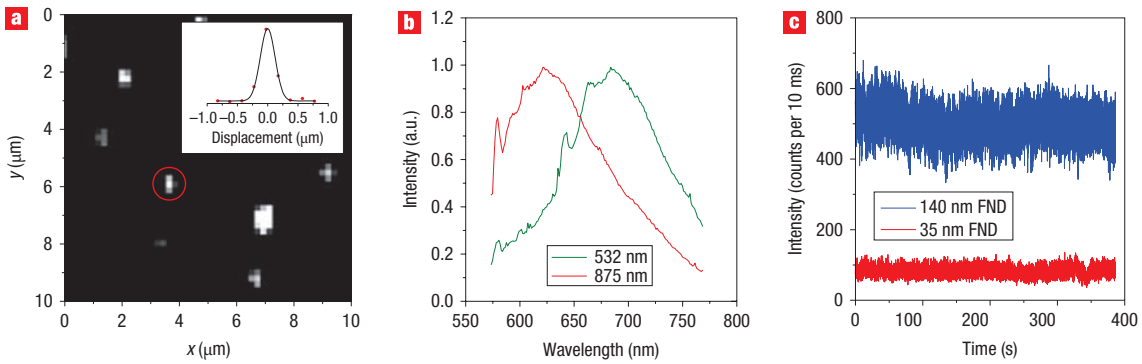

Figure 2 Two-photon excited fluorescence of FNDs. a, TPE fluorescence image of 140-nm FNDs dispersed on a cover-glass slide. Inset: Image profile of the single FND particle circled in red. **b**, Comparison of fluorescence spectra of a single 140-nm FND excited with 532-nm photons for OPE and 875-nm photons for TPE. **c**, Photostability tests of a single 35-nm FND and a single 140-nm FND upon TPE with a femtosecond Ti-sapphire laser at average powers of 7.0 mW and 2.4 mW, respectively.

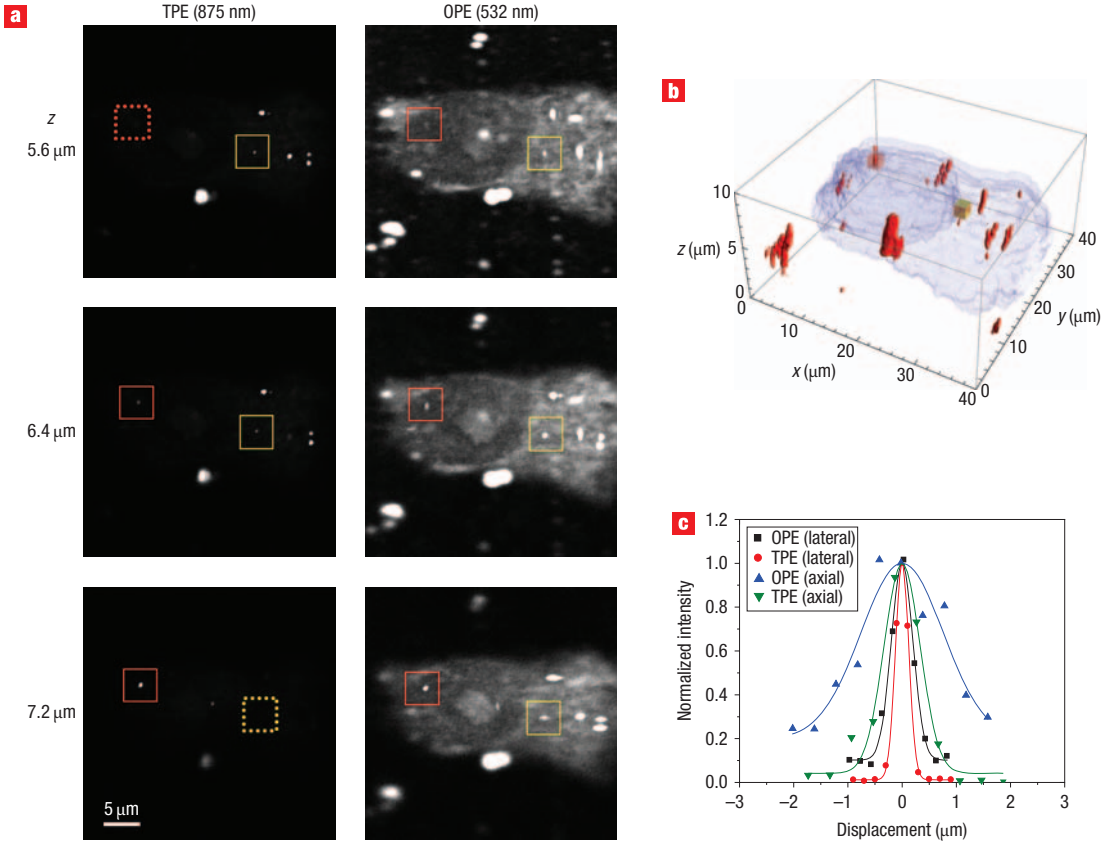

Figure 3 One-photon and two-photon excited fluorescence images of 140-nm FNDs in a fixed HeLa cell. a, OPE and TPE confocal fluorescence images of the same cell. **b**, Three-dimensional TPE image of the cell and the internalized FNDs. **c**, Lateral and axial cross-sections of the FND labelled with a red box in **a**. Note that the resolution of TPE for this particular particle was ~300 nm in the lateral direction and ~800 nm in the axial direction, both of which are close to their theoretical diffraction limits.

in a wide-field mode (see Supplementary Information, Figs S7 and S8), we were able to track a single FND (marked with a yellow box in Fig. 4a) inside the cell over a timespan of more than 200 s. From a mean square displacement analysis[27] of the three-dimensional trajectory (Fig. 4b), we determined a diffusion coefficient of 3.1×10^{-3} $\mu m^2 s^{-1}$ for the internalized FND particle. This value is in good agreement with reported diffusion coefficients of quantum dots confined within an endosome[24].

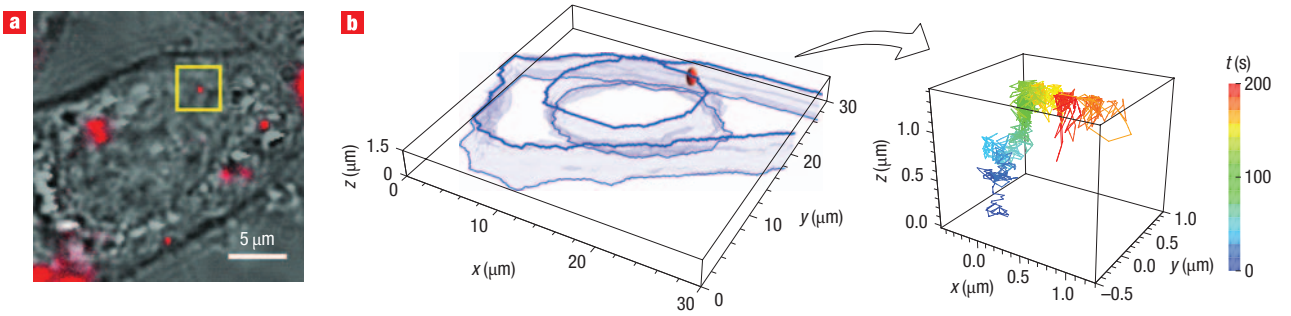

Figure 4 Three-dimensional tracking of a single 35-nm FND in a live HeLa cell. a, Bright-field and epifluorescence (red pseudo-colour) images of the cell after FND uptake. **b**, Three-dimensional reconstruction (left panel), showing the boundaries of the nucleus and the cytoplasm of the cell. Three-dimensional trajectory (shown in pseudo-colour, right panel) and displacements of a single FND (labelled with a yellow box in **a**) inside the cell over a time span of 200 s. (See Supplementary Information, Fig. S9, for a figure showing the (*x*,*y*) displacements, and Movie S2 for a video showing the real-time motion of the FND.).

To conclude, we have developed a practical method for the production of FND in quantity. Compared with organic fluorophores whose time-lapse imaging is limited by photobleaching[28], FND as a nanoprobe provides an excellent opportunity to follow both fast (ms) and slow (h) events in cells, tissues and even small animals. Integrating the existing and emerging nanodiamond technologies[1–4,8,13,17,29,30] into practice is expected to open up exciting new horizons for applications of this novel material in nanomedicine and nanobiology.

METHODS

Synthetic type Ib diamond powders with a mean particle diameter of 35 nm and 140 nm were obtained from Microdiamant (Switzerland) and Element Six (USA), respectively. They typically contain 100 p.p.m. of atomically dispersed nitrogen atoms as the major internal impurity. Radiation damage of the nanocrystallites by 40-keV He+ bombardment was conducted with an ion beam generated by discharge of pure He in a radio-frequency positive ion source (National Electrostatics Corporation) and guided by a high-voltage acceleration tube in a vacuum chamber built in-house. Mass production of FNDs was made by depositing nanodiamond powders on a long copper tape to form a thin film (~0.2 μm thick), followed by insertion of the tape in the beam path and winding the tape inside the vacuum chamber using an external stepper motor. Predominantly negatively charged nitrogen-vacancy, $(N\text{-}V)^-$, centres formed upon annealing of the irradiated nanocrystallites at 800 °C for 2 h (ref. 14).

TPE experiments were conducted with a setup consisting of a modified stage-scanning confocal fluorescence microscope (E600, Nikon) coupled with a femtosecond mode-locked Ti-sapphire laser (Mira 900, Coherent). The same setup was also adapted for OPE measurements using a cw 532-nm laser as the excitation source, along with a different set of filters and dichroic mirrors. To overcome the stage instability in long-term (>1 h) three-dimensional imaging of whole cells, a method taking advantage of the photostability of FND was developed. Using a FND particle in the sample as the reference point, a subroutine in the scanning program periodically guided the stage to go back and forth to check the position of that particular particle and compensate for any drift errors that might arise during sample scanning.

Three-dimensional single-particle tracking of FNDs in live cells was performed with an automated wide-field fluorescence microscope (IX-71, Olympus). The system was designed in such a way that it monitored continuously the real-time position of the nanoprobe in three dimensions and tracked its motion according to the changes in intensity and shape of the epifluorescence image. A feedback servo control constantly retained the probe within the depth of field of the microscope objective. Before the cell experiment, the performance of this home-built system was tested by tracking single dye-doped polystyrene beads as well as FNDs in a glycerol–water solution.

The procedures for preparing single FNDs on a cover-glass slide, a culture of HeLa cells and cellular uptake of FNDs have been described previously[1,2]. Further details of the experimental setups, single-particle fluorescence spectra, time-trace measurements, as well as performance tests of the three-dimensional single-particle tracking system can be found in the Supplementary Information.

Received 28 February 2008; accepted 3 April 2008; published 27 April 2008.

References

1. Yu, S.-J., Kang, M.-W., Chang, H.-C., Chen, K.-M. & Yu, Y.-C. Bright fluorescent nanodiamonds: No photobleaching and low cytotoxicity. *J. Am. Chem. Soc.* **127,** 17604–17605 (2005).
2. Fu, C.-C. *et al.* Characterization and application of single fluorescent nanodiamonds as cellular biomarkers. *Proc. Natl Acad. Sci. USA* **104,** 727–732 (2007).
3. Huang, L.-C. L. & Chang, H.-C. Adsorption and immobilization of cytochrome *c* on nanodiamonds. *Langmuir* **20,** 5879–5884 (2004).
4. Neugart, F. *et al.* Dynamics of diamond nanoparticles in solution and cells. *Nano Lett.* **7,** 3588–3591 (2007).
5. Akin, D. *et al.* Bacteria-mediated delivery of nanoparticles and cargo into cells. *Nature Nanotech.* **2,** 441–449 (2007).
6. Medintz, I. L., Uyeda, H. T., Goldman, E. R. & Mattoussi, H. Quantum dot bioconjugates for imaging, labelling and sensing. *Nature Mater.* **4,** 435–446 (2005).
7. Cui, B. *et al.* One at a time, live tracking of NGF axonal transport using quantum dots. *Proc. Natl Acad. Sci. USA* **104,** 13666–13671 (2007).
8. Gruber, A. *et al.* Scanning confocal optical microscopy and magnetic resonance on single defect centres. *Science* **276,** 2012–2014 (1997).
9. Treussart, F. *et al.* Photoluminescence of single colour defects in 50 nm diamond nanocrystals. *Physica B* **376,** 926–929 (2006).
10. Schrand, A. M. *et al.* Are diamond nanoparticles cytotoxic? *J. Phys. Chem. B* **111,** 2–7 (2007).
11. Liu, K,-K., Cheng, C.-L., Chang, C.-C. & Chao, J.-I. Biocompatible and detectable carboxylated nanodiamond on human cell. *Nanotechology* **18,** 325102 (2007).
12. Huang, H., Pierstorff, E., Osawa, E. & Ho, D. Active nanodiamond hydrogels for chemotherapeutic delivery. *Nano Lett.* **7,** 3305–3314 (2007).
13. Schrand, A. M., Dai, L. M., Schlager, J. J., Hussain, S.M. & Osawa, E. Differential biocompatibility of carbon nanotubes and nanodiamonds. *Diamond Relat. Mater.* **16,** 2118–2123 (2007).
14. Davies, G. & Hamer, M. F. Optical studies of 1.945 eV vibronic band in diamond. *Proc. R. Soc. Lond. A* **348,** 285–298 (1976).
15. Lawson, S. C., Fisher, D., Hunt, D. C. & Newton, M. On the existence of positively charged single-substitutional nitrogen in diamond. *J. Phys. Condens. Matter* **10,** 6171–6180 (1998).
16. Ziegler, J. F., Biersack, J. P. & Littmark, U. *The Stopping and Range of Ions in Solids* (Pergamon, New York, 1985).
17. Wee, T.-L. *et al.* Two-photon excited fluorescence of nitrogen-vacancy centers in proton-irradiated type Ib diamond. *J. Phys. Chem. A* **111,** 9379–9386 (2007).
18. Xu, C., Zipfel, W., Shear, J. B., Williams, R. M. & Webb, W. W. Multiphoton fluorescence excitation: New spectral windows for biological nonlinear microscopy. *Proc. Natl Acad. Sci. USA* **93,** 10763–10768 (1996).
19. Helmchen, F. & Denk, W. Deep tissue two-photon microscopy. *Nature Methods* **2,** 932–940 (2005).
20. Vlasov, I. I. *et al.* Relative abundance of single and vacancy-bonded substitutional nitrogen in CVD diamond. *Phys. Stat. Sol. A* **181,** 83–90 (2000).
21. Dumeige, Y. *et al.* Photo-induced creation of nitrogen-related color centers in diamond nanocrystals under femtosecond illumination. *J. Luminesc.* **109,** 61–67 (2004).
22. Gu, M. in *Principle of Three-Dimensional Imaging in Confocal Microscopes* Ch. 5 (World Scientific, Singapore, 1996).
23. Speidel, M., Jonas, A. & Florin, E.-L. Three-dimensional tracking of fluorescent nanoparticles with subnanometer precision by use of off-focus imaging. *Opt. Lett.* **28,** 69–71 (2003).
24. Holtzer, L., Meckel, T. & Schmidt, T. Nanometric three-dimensional tracking of individual quantum dots in cells. *Appl. Phys. Lett.* **90,** 053902 (2007).
25. Cang, H., Xu, C. S., Montiel, D. & Yang, H. Guiding a confocal microscope by single fluorescent nanoparticles. *Opt. Lett.* **32,** 2729–2731 (2007).
26. Greber, U. F. & Way, M. A superhighway to virus infection. *Cell* **124,** 741–754 (2006).
27. Hong, Q. A., Sheetz, M. P. & Elson, E. L. Single-particle tracking—analysis of diffusion and flow in 2-dimensional systems. *Biophys. J.* **60,** 910–921 (1991).
28. Yu, J., Xiao, J., Ren, X., Lao, X. & Xie, X. S. Probing gene expression in live cells, one protein molecule at a time. *Science* **311,** 1600–1603 (2006).

29. Krüger, A., Liang, Y. J., Jarre, G. & Stegk, J. Surface functionalisation of detonation diamond suitable for biological applications. *J. Mater. Chem.***16,** 2322–2328 (2006).
30. Smith, B. R., Niebert, M., Plakhotnik, T. & Zvyagin, A. V. Transfection and imaging of diamond nanocrystals as scattering optical labels. *J. Luminesc.* **127,** 260–263 (2007).

Supplementary Information accompanies this paper at www.nature.com/naturenanotechnology.

Acknowledgements

This work was supported by the Academia Sinica and the National Science Council (grant no. NSC 96-2120-M-001-008 and NSC-95-2120-M-002-003) of Taiwan, ROC.

Author contributions

H.-C.C. and W.F. conceived and designed the experiments. Y.-R.C., H.-Y.L., K.C., C.-C.C., D.-S.T., C.-C.F., T.-S.L., Y.-K.T. and C.-Y.F. performed the experiments. Y.-R.C., H.-Y.L., C.-Y.F., H.-C.C. and W.F. analysed the data. C.-C.H. contributed materials and analysis tools. Y.-R.C., H.-C.C. and W.F. co-wrote the paper. Y.-K.T. and C.-Y.F. are responsible for mass production, H.-Y.L. and C.-C.C. are responsible for two-photon imaging, Y.-R.C., C.-C.F., D.-S.T. and K.C. are responsible for three-dimensional tracking of FNDs.

Author information

Reprints and permission information is available online at http://npg.nature.com/reprintsandpermissions/.
Correspondence and requests for materials should be addressed to H.-C.C. and W.F.